EURASIP Journal on Applied Signal Processing 2004:16, 2423–2433

Impulsive Noise Suppression from Images by Using Anfis Interpolant and Lillietest

Erkan Beşdok

Computer Engineering Department, Institute of Science, Erciyes University, 38039 Kayseri, Turkey
Email: ebesdok@erciyes.edu.tr

Received 14 July 2003; Revised 30 January 2004

A new impulsive noise (IN) elimination filter, entitled adaptive neuro-fuzzy inference system-based IN removal filter (*Anfis-F*), which shows high performance at the restoration of images distorted by IN, is proposed in this paper. The *Anfis-F* comprises three main steps: finding the pixels that are suspected to be corrupted, the Delaunay triangulation, and finally, making estimation for intensity values of corrupted pixels within each of the Delaunay triangles. Extensive simulation results show that the proposed filter achieves better performance than other filters mentioned in this paper in the cases of being effective in noise suppression and detail preservation, especially when the noise density is very high.

Keywords and phrases: impulsive noise suppression, finite-element-based Anfis, Delaunay triangulation.

1. INTRODUCTION

Image enhancement and noise filtering are the most common tasks in image processing. Images are affected by impulsive noise (IN) during image acquisition, transmission, or storage; therefore noise-free images are rare in the real world. Noise suppression of distorted images requires a balance between the gained improvement and the introduced degradation by a particular filter. Preservation of image details while eliminating IN is usually not possible during the noise suppression process, but both of them are crucial for the subsequent processing stages.

It has been approved that the standard median filter (SMF) [1], as well as its modifications and generalizations, [2, 3, 4, 5, 6, 7, 8], offers satisfying performance in suppression of IN. However, these approaches are implemented invariantly across the image, thus they tend to alter the pixels undisturbed by IN and increase the edge jitters when the noise ratio is high. Consequently, achieving a good performance in the suppression of IN is usually at the expense of blurred and distorted image features. One way to avoid this problem is to include a decision-making component in the filtering structure based on very simple, but effective, impulse detection (ID) mechanism. The function of the ID mechanism is to check each pixel to detect whether it is distorted or not. Then, the nonlinear filtering scheme is achieved for the distorted pixels, while the noise-free pixels are left unaltered in order to avoid excessive distortion. Recently, such ID-based median filtering methods with thresholding operations have been realized by using different modifications of impulse detectors where the output is switched between the identities or median-based filtering scheme [2, 4, 6, 7].

The *Anfis-F*, proposed in this paper, differs from the other median-based filters by performing the restoration of degraded images with high performance according to both subjective measures (e.g., visually pleasing) and objective measures (e.g., mean squared error (MSE)) even if the images have been highly corrupted by IN.

The theories of the fuzzy set and *neural paradigm* have been greatly used in the field of image processing since they were proposed. It is apparent that a combination of the fuzzy and neural paradigms can play a very important role in the processing of signals because the well understandable structure of fuzzy knowledge can be discovered from a set of training data. The neuro-fuzzy approach is in fact very effective for system modeling and information processing because of its ability to approximate complex nonlinear functions and this paper proposes a new filter based on adaptive neuro-fuzzy inference system (Anfis) theory. The performance of the proposed filter is compared with SMF [1], iterative median filter (IMF) [2], and the recently introduced complex structured IN removal filters: progressive switching median filter (PSM) [2], signal-dependent rank order mean filter (SDROM) [5], two-state recursive signal-dependent rank order mean filter (SDROMR) [5], impulse rejecting filter (IRF) [7], nonrecursive adaptive center weighted median filter (ACWM) [4], recursive adaptive center weighted median filter (ACWMR) [4], center weighted median filter (CWM) [6], recursive center weighted median filter (CWMR) [9],

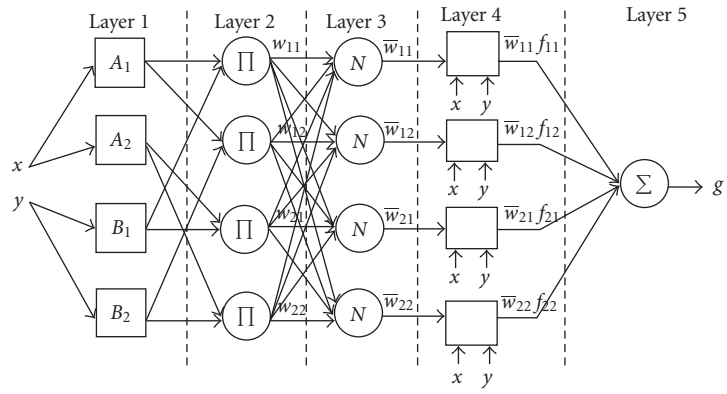

Figure 1: The Anfis structure used in the proposed method.

selective median filter (SSMF) [10], and Yüksel's Anfis-based fuzzy filter (YUKSEL) [11].

The rest of the paper is organized as follows. The details of the Anfis and finite-element-based soft computing is given in Section 2. Using Delaunay triangles as finite elements is given in Section 3. Analyzing impulsive behavior of the pixels by using lillietest is mentioned in Section 4. The proposed method is defined in Section 5 and, finally, experiments and conclusions are presented in Sections 6 and 7, respectively.

2. ANFIS AND FINITE-ELEMENT-BASED SOFT COMPUTING

In the last few years, soft-computing techniques (artificial neural networks, fuzzy systems, genetic algorithms, etc.) have been successfully applied in the area of image processing [10, 11, 12, 13, 14, 15, 16]. Soft-computing techniques are in fact very effective for image processing because of their ability to approximate complex nonlinear functions [17, 18, 19, 20, 21]. A key advantage of the Anfis is its use in the representation of image information. Therefore, Anfis [17, 18] has been used in this paper in order to remove IN from distorted images.

2.1. Anfis

Neuro-fuzzy systems [17, 18] are hybrids of fuzzy systems [12, 13, 14, 15, 16, 17, 18, 19, 20, 21, 22] and neural networks [23, 24, 25]. The goal of neuro-fuzzy systems is to combine the learning capability of a neural network with the intuitive representation of knowledge found in a fuzzy system. This may be accomplished by designing a network architecture to mimic a fuzzy system, by incorporating linguistic terms into the computations performed by the network, by means of an explanation mechanism for the network, and so forth. Anfis is the well-known neuro-fuzzy system, which mimics the operation of a Takagi-Sugeno-Kang (TSK) fuzzy system [20, 21]. The mathematical details of the Anfis have been given in [17, 25]. The Anfis network is a five-layered network, in which the layers are not fully connected. The transfer function of a neuron is determined according to the layer where the neuron is.

All the Anfis structures used in this paper (Figure 1) possess two inputs (x, y) and one output (g). Here, (x, y) and g denote the spatial positions of the corner nodes and the intensity (gray) values at the corner nodes of the related Delaunay triangles [25, 26, 27, 28, 29, 30] (Figure 2), respectively. Each input of the Anfis structures has 2 different triangular membership functions and the rule base contains a total of 4 (2^2) rules, which are as follows:

(i) Rule 1: if x is A_1 and y is B_1, then $f_{11} = p_{11}x + q_{11}y + r_{11}$,

(ii) Rule 2: if x is A_1 and y is B_2, then $f_{12} = p_{12}x + q_{12}y + r_{12}$,

(iii) Rule 3: if x is A_2 and y is B_1, then $f_{21} = p_{21}x + q_{21}y + r_{21}$,

(iv) Rule 4: if x is A_2 and y is B_2, then $f_{22} = p_{22}x + q_{22}y + r_{22}$,

where p, q, and r denote the consequent parameters [17, 25].

The parameters of membership functions were obtained for each Delaunay triangle [25, 26, 27, 28, 29, 30] by training the Anfis structures with 10 epochs. At the training phase of the fuzzy structures, a combination of least squares and back-propagation gradient descent methods [17, 25] is used, in order to compute the parameters of the membership functions, which are used to model given set of inputs (x, y) and single-output data "g." The computational detail of Anfis structures is given below.

Let the membership functions of fuzzy sets A_i and B_j, be μ_{A_i} and μ_{B_j}, respectively, where $i = 1, 2$ and $j = 1, 2$.

(i) Layer 1:

$$\mu_{A_i}(x) = \max\left(\min\left(\frac{x - a_i}{b_i - a_i}, \frac{c_i - x}{c_i - b_i}\right), 0\right),$$
$$\mu_{B_j}(y) = \max\left(\min\left(\frac{y - a_j}{b_j - a_j}, \frac{c_j - y}{c_j - b_j}\right), 0\right), \quad (1)$$

where $\mu_{A_i}(x)$ and $\mu_{B_j}(y)$ were chosen as triangular membership functions [25] with the parameters of a, b, and c.

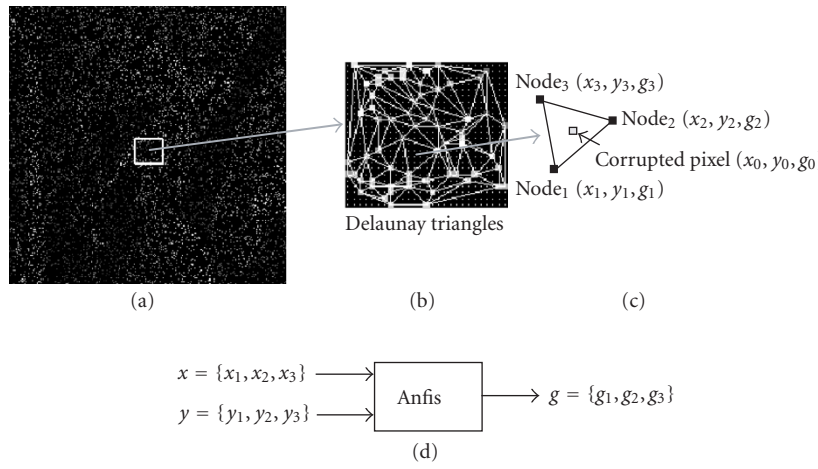

Figure 2: The relations between the corrupted image, Delaunay triangulation, and the Anfis structure. (a) The corrupted Lena image at the noise density of 90% (corrupted pixels have been represented as black for illustration). (b) Delaunay network over the noisy image (the corner nodes of the Delaunay triangles are uncorrupted pixels of the corrupted image). (c) One of the Delaunay triangles given in detail. (d) The Anfis structure, which has been used in this paper.

(ii) Layer 2:

$$w_{ij} = \mu_{A_i}(x)\mu_{B_j}(y). \tag{2}$$

The logical operation *and* has been used as *product* [17, 25] for all the rules.

(iii) Layer 3:

$$\overline{w}_{ij} = \frac{w_{ij}}{w_{11} + w_{12} + w_{21} + w_{22}}. \tag{3}$$

(iv) Layer 4: every node in this layer is a square node with a linear function [17, 25] (η_{ij}) as

$$\eta_{ij} = \overline{w}_{ij} f_{ij} = \overline{w}_{ij}(p_{ij}x + q_{ij}y + r_{ij}). \tag{4}$$

(v) Layer 5: the single node in this layer is labeled with $\sum$, which computes the overall output, g, as the summation of all incoming signals, that is,

$$g = \sum_{i=1}^{2}\sum_{j=1}^{2} \eta_{ij}. \tag{5}$$

2.2. Finite-element-based soft computing

The proposed method benefits from finite-element computing [30] in making estimation for gray values of the corrupted pixels. In this paper, Delaunay triangular finite elements have been used.

Surface fitting is a useful tool for preserving huge amount of information in the spatial data [26, 27, 28, 29, 30]. An image surface is a representation of the pixel values that are continuous over image space and image surfaces can be created to represent any kind of measure of thematic information, such as topographic elevation, spatial temperature, or spatial intensity of electromagnetic field [27].

Descriptive surface fitting (DSF) methods are the most commonly used methods for surface fitting [26, 27, 28, 29, 30]. The DSF methods do not use statistical models and do not explicitly recognize spatial dependence [26, 27, 28, 29, 30]. Furthermore, error estimates cannot be achieved in DSF methods and predictions for corrupted pixel values with the lowest error cannot be produced [27]. Therefore, DSF methods are really exploratory methods for image surfaces, not formal predictors. In real-time applications, the DSF methods are often used for prediction of surfaces, due to their ease of use and simplicity in computational requirements. There are many techniques introduced to create DSF surfaces [26, 27, 28, 29, 30].

In real images, pixels do not scatter randomly. Therefore, the gray value of a pixel is more related to the neighboring pixels than distant ones. The restoration of image surface from the data of uncorrupted pixels is based on this observation, which is a reflection of the spatial dependence of the uncorrupted pixels in real images. Since TSK fuzzy models are universal approximators and provide good interpolation and extrapolation characteristics [20, 21], Anfis, which is based on TSK fuzzy model, has been preferred in this paper in order to interpolate the restored values of the corrupted pixels.

3. USING DELAUNAY TRIANGLES AS FINITE ELEMENTS

Delaunay triangulation [25, 26, 27, 28, 29, 30] is a fundamental and well-studied problem in computational geometry and it is commonly used as finite elements in the literature [30]. In this study, Delaunay triangulation is defined within the convex hull [25] of the uncorrupted pixels as a set of triangles with the following five properties:

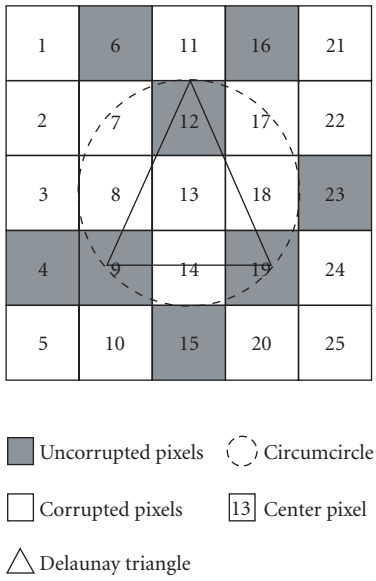

Figure 3: The relation among the Delaunay triangle, corrupted pixels, and uncorrupted pixels.

(i) the triangle vertices are corner nodes, which are members of the set of uncorrupted pixels,
(ii) no triangle contains a corner node other than its vertices,
(iii) the interiors of the triangles are pairwise disjointed,
(iv) the union of triangles is the convex hull of the set of corner nodes,
(v) the interior of the circumcircle of each triangle contains no corner node.

Delaunay triangles have been used in solving some problems on simulation of the growth of crystals, cartography, photogrammetry, city planning, computational geometry, mesh generation for finite elements methods, visualization of surfaces, and image processing [25, 26, 27, 28, 29, 30]. The geometric definition of the Delaunay triangulation has been illustrated in Figure 3.

4. ANALYZING IMPULSIVE BEHAVIOR OF THE PIXELS BY USING LILLIETEST

Statistical methods are useful tools for analyzing impulsive behavior of the pixels within the real images [31]. Extensive simulations exposed that each intensity level within the real images possesses at least one best-fitted statistical distribution model. For the study proposed in this paper, 30 statistical distribution models have been examined and all of them have been implemented in Matlab [25], in order to find out the best-fitted distribution statistical model for each of the intensity levels. The examined distribution models are given in Figure 4. This statistical analysis has revealed that the well-known normal distribution model [25, 32, 33, 34] appears to be the best statistical distribution model for the sample of intensity data, which are derived from 32×32 pixel-sized unoverlapping blocks (bins) as explained below and seen in Figure 5.

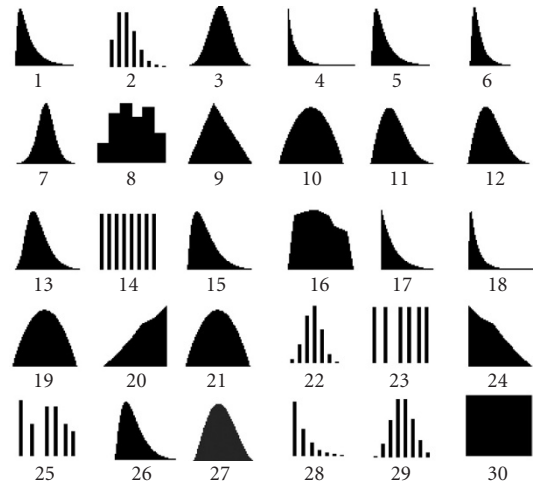

Figure 4: The probability distribution models of the examined distributions: (1) logarithmic normal, (2) Poisson, (3) normal, (4) Pareto, (5) logarithmic normal (continuous), (6) Pearson, (7) T-student, (8) histogram, (9) triangular, (10) Beta, (11) Rayleigh, (12) Weibull, (13) exterme value, (14) integer uniform, (15) Gamma, (16) general, (17) exponential, (18) inverse Gaussian, (19) Beta general, (20) cumulative (ascending), (21) Beta subjective, (22) hypergeometric, (23) discrete uniform, (24) cumulative (descending), (25) discrete, (26) Chi-squared, (27) Pert (beta), (28) geometric, (29) binomial, and (30) uniform.

The lillietest (Lilliefors test) [25, 33, 34], evaluates the hypothesis that the sample has a normal distribution with unspecified mean and variance against the alternative hypothesis that the sample does not have a normal distribution. Lillietest is generally more relevant than the commonly used statistical tests (e.g., Kolmogorov-Semirnov test [25, 32, 33]) because of its computational structure.

The lillietest statistic is computed from the maximum vertical offset of the empirical cumulative distribution functions (CDFs) [25, 33] of the sample, after conversion to Z-scores [25, 33], and the standard normal distribution. A sample is converted to Z-scores by subtracting the sample mean and dividing by the sample standard deviation, so that the mean of the Z-score series is 0 and the standard deviation is 1.000. The empirical CDF of this Z-score series is computed. The details of the lillietest is given below [25, 33].

Data

U samples are considered as $\underline{X}_g = \{X_0, X_1, X_2, \ldots, X_U\}$ for the intensity levels, $g = 0, 1, 2, \ldots, 255$. The corrupted image plane is divided into 32×32 pixel-sized unoverlapping blocks (bins) (as seen in Figure 5), in order to count the number of the g within each block. Therefore, totally 64 blocks have been obtained for 256×256 pixel-sized test images and $U = 64$. Each element of the $\underline{X}_g$ corresponds to the numbers of the g within each of the blocks. The distribution function of the set $\underline{X}_g$ is denoted by Q. The sample mean, λ, and sample standard deviation, σ, are computed and then the sample is

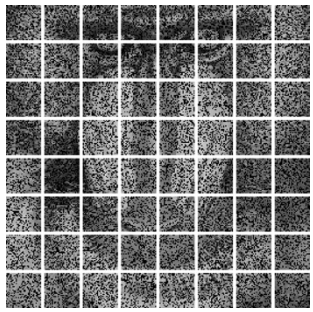

(a)

(b)

Figure 5: Searching the corrupted pixels for the Mandrill image which is at the noise density of 30%. (a) The 32×32 pixel-sized blocks (bins) over the corrupted image (the corrupted pixels were marked as black for illustration). (b) The corrupted image where the corrupted pixels were derived by using lillietest and were marked as black for illustration.

converted to Z-scores as

$$Z_h = \frac{X_h - \lambda}{\sigma}, \quad h = 0, 2, 3, \ldots, U. \tag{6}$$

Assumption

It is assumed that $\underline{X}_g$ is a sample set of the observations $\underline{X}_g = \{X_0, X_1, X_2, \ldots, X_U\}$, which are not independent from another. This assumption is essential for modeling the spatial uniformity of real images.

Hypotheses

(H_0) The distribution function of the $\underline{X}_g$ is normal distribution with unspecified mean and variance.

(H_1) The distribution function of $\underline{X}_g$ is abnormal.

Test statistics

The test statistics of the lillietest is the maximum vertical distance between the empirical distribution function of the Z-score series in (7) and the distribution function of the standard normal distribution is given as

$$T = \sup \left| Q^* - S \right|, \tag{7}$$

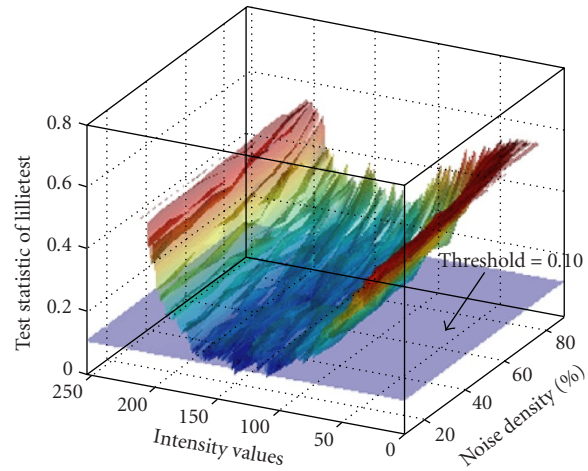

Figure 6: Test statistics of lillietest for the corrupted Mandrill test images.

where Q^* and S denote the CDF of the standard normal distribution and the empirical CDF of the Z-scores, respectively. Extensive simulations show that the value of the lillietest statistics, T, smaller than 0.10 ± 0.05 corresponds to abnormally distributed intensity levels in real images.

The test statistics of the lillietest for the Mandrill test image is illustrated in Figure 6. Abnormally distributed intensity values were assumed to be corrupted pixels in this paper and extensive simulations verified this assumption as seen in the results of the experiments (Tables 1, 2, and 3, and Figures 7–10).

Decision rule

Reject (H_0) at the significance level if T exceeds $(1-\alpha)$, where α denotes *the significance level* of the test and $\alpha = 0.05$ [33].

5. PROPOSED METHOD

The proposed filter, *Anfis-F*, is a finite-element-based filter and uses Delaunay triangles (as seen in Figures 2 and 3) as finite elements. The *Anfis-F* comprises three main steps: finding the pixels that are suspected to be corrupted, Delaunay triangulation, and making estimation for intensity values of corrupted pixels. For the implementation of *Anfis-F*, the distorted image was padded with 5 pixels reflected copy of itself on the sides in order to cover the whole image with Delaunay triangulation network. The triangulation phase was achieved by using the spatial positions of the abnormally distributed intensity levels. The convex hull and Delaunay triangles were both obtained over the image after the Delaunay triangulation phase as expressed in Section 3.

The abnormally distributed intensity levels within the corrupted image were determined by using lillietest, as explained in Section 4. After the Delaunay triangulation phase, the Delaunay triangles, which do not consist at least one corrupted pixel, were deleted in order to reduce computational cost of *Anfis-F*. Delaunay triangles encompass the most likely corrupted pixels because the corner nodes of the Delaunay triangles are centered at uncorrupted pixels.

Table 1: The restoration results for Lena test image in respect of MSE.

Method	Noise density								
	10%	20%	30%	40%	50%	60%	70%	80%	90%
Noisy image	1852.70	3767.60	5563.60	7451.50	9268.40	11152.00	13078.00	14769.00	16804.00
Anfis-F	**13.47**	**26.76**	**49.60**	**75.36**	**114.16**	**154.95**	**205.15**	**278.50**	**385.89**
IMF	124.05	140.06	158.84	203.36	261.87	491.57	1402.70	3971.50	10140.00
SMF	87.09	148.82	353.46	958.83	2046.10	3856.60	6769.10	9938.00	14269.00
PSM	54.92	85.76	132.48	272.63	647.30	1938.30	5036.00	9495.10	14862.00
SDROM	60.52	136.35	408.80	1105.70	2339.10	4322.30	7404.70	10619.00	14831.00
SDROMR	56.79	91.21	171.88	287.33	553.76	1071.80	2452.10	5615.90	13152.00
IRF	61.15	127.84	366.24	981.06	2098.80	3918.50	6821.70	9982.40	14290.00
ACWM	51.97	121.51	367.27	993.73	2119.40	3951.00	6859.10	10015.00	14311.00
ACWMR	46.95	85.67	170.71	299.57	536.23	1007.80	2042.30	4230.20	9975.40
CWM	76.27	259.94	727.17	1729.30	3273.40	5431.60	8350.40	11291.00	15060.00
CWMR	586.89	662.15	962.16	1550.30	2750.50	4539.70	6943.40	9950.80	13190.00
SSMF	88.47	159.34	415.68	1000.00	2288.50	4369.80	7236.40	11026.00	15283.00
YUKSEL	397.60	519.93	696.40	932.45	1229.00	1611.90	2091.90	2704.10	3433.80

Table 2: The restoration results for Mandrill test image in respect of MSE.

Method	Noise Density								
	10%	20%	30%	40%	50%	60%	70%	80%	90%
Noisy image	1766.50	3585.30	5351.70	7093.50	8898.20	10623.00	12415.00	14201.00	15998.00
Anfis-F	**32.55**	**70.49**	**114.15**	**165.16**	**221.13**	**294.10**	**371.94**	**462.27**	**600.31**
IMF	324.10	340.02	358.99	386.60	456.02	657.79	1653.40	4082.50	9688.00
SMF	271.04	329.47	560.00	1094.30	2184.30	3836.80	6583.00	9739.10	13720.00
PSM	108.39	147.80	205.12	335.73	736.27	1932.40	5146.60	9665.40	14527.00
SDROM	165.39	259.65	544.67	1187.70	2443.10	4264.30	7185.30	10451.00	14272.00
SDROMR	171.74	224.09	312.82	429.68	692.46	1122.90	2482.90	5432.60	12614.00
IRF	171.56	252.63	497.92	1071.00	2190.20	3856.00	6614.30	9786.60	13742.00
ACWM	125.94	215.00	470.31	1052.30	2180.10	3851.70	6620.20	9798.60	13749.00
ACWMR	115.20	176.27	263.32	381.32	620.87	975.77	1888.50	3713.40	8619.00
CWM	184.00	348.50	836.76	1795.20	3319.70	5272.30	8037.50	10960.00	14346.00
CWMR	436.04	524.33	803.14	1356.30	2407.60	3980.50	6161.00	8760.20	11555.00
SSMF	206.63	269.15	493.26	1017.60	2120.60	3899.20	6462.20	9807.10	13570.00
YUKSEL	44.13	83.68	143.72	235.90	363.89	547.14	787.89	1118.30	1534.10

Anfis was used as an interpolant for each Delaunay triangle in order to get the estimated gray values of corrupted pixels, which are encompassed by the related Delaunay triangle. Then, the original gray values of the normally distributed pixels and the estimated gray values of the corrupted pixels were reorganized in order to obtain the restored image. For the computation of restored gray values of corrupted pixels; this paper offers using an Anfis, whose structure is shown in Figure 1, as a DSF interpolant [27, 28, 29, 30] for each Delaunay triangle. DSF-based applications of the supervised fuzzy systems do not need using verification data [25] in their training (e.g., as in [11, 35]), in order to produce good results. The final result is more important than local verifications of data for DSF interpolants.

Since Anfis has been used as a DSF interpolant for each Delaunay triangle, only training data set has been enough to solve our problem, as in [11, 35]. The structure of the Delaunay network changes with the intensity of the noise density in distorted image, therefore a specific learning phase is required whenever a new corrupted image is presented.

The training phase of the Anfis structure is visually explained in Figure 2. Each Delaunay triangle includes at least one corrupted pixel and the number of the Delaunay triangles corresponds to the number of the Anfis structures that are needed to be trained. In order to explain the proposed method more coherently, the computational algorithm of the *Anfis-F* is given below step by step.

(i) Pad the image with 5 pixels reflected copy of itself on the sides in order to cover the whole image with Delaunay network.

(ii) Find the spatial image coordinates, (x, y), of the abnormally distributed pixels, which were determined by using lillietest statistics.

Table 3: The restoration results for Peppers test image in respect of MSE.

Method	Noise density								
	10%	20%	30%	40%	50%	60%	70%	80%	90%
Noisy image	1940.10	3988.80	5897.70	7914.50	9960.80	11929.00	13993.00	15930.00	17908.00
Anfis-F	**13.19**	**29.65**	**53.17**	**84.66**	**124.42**	**172.13**	**234.00**	**332.78**	**488.56**
IMF	123.82	149.80	190.54	249.05	335.41	667.77	1693.60	4329.20	10742.00
SMF	77.69	160.17	389.36	1021.90	2161.00	4151.50	7271.20	10690.00	15164.00
PSM	55.24	94.58	159.79	301.41	714.25	1952.20	5280.30	9673.30	15099.00
SDROM	63.70	195.43	482.43	1240.30	2528.90	4674.00	7960.80	11444.00	15787.00
SDROMR	61.34	149.97	268.08	474.06	750.02	1568.00	3167.30	6270.00	13218.00
IRF	60.14	182.08	437.96	1126.40	2299.90	4309.50	7444.10	10835.00	15306.00
ACWM	55.70	181.99	442.58	1139.30	2317.90	4333.40	7471.50	10859.00	15324.00
ACWMR	54.51	142.14	259.92	463.44	727.67	1395.30	2753.00	4820.70	10357.00
CWM	84.55	303.75	818.32	1860.70	3557.80	5858.40	8999.30	12226.00	16049.00
CWMR	298.04	375.45	645.59	1200.00	2281.40	3958.70	6310.80	9158.70	12313.00
SSMF	29.67	82.28	302.77	838.66	2005.70	3922.20	6687.50	10286.00	14384.00
YUKSEL	97.46	144.16	227.19	360.70	559.04	843.88	1217.80	1713.90	2350.80

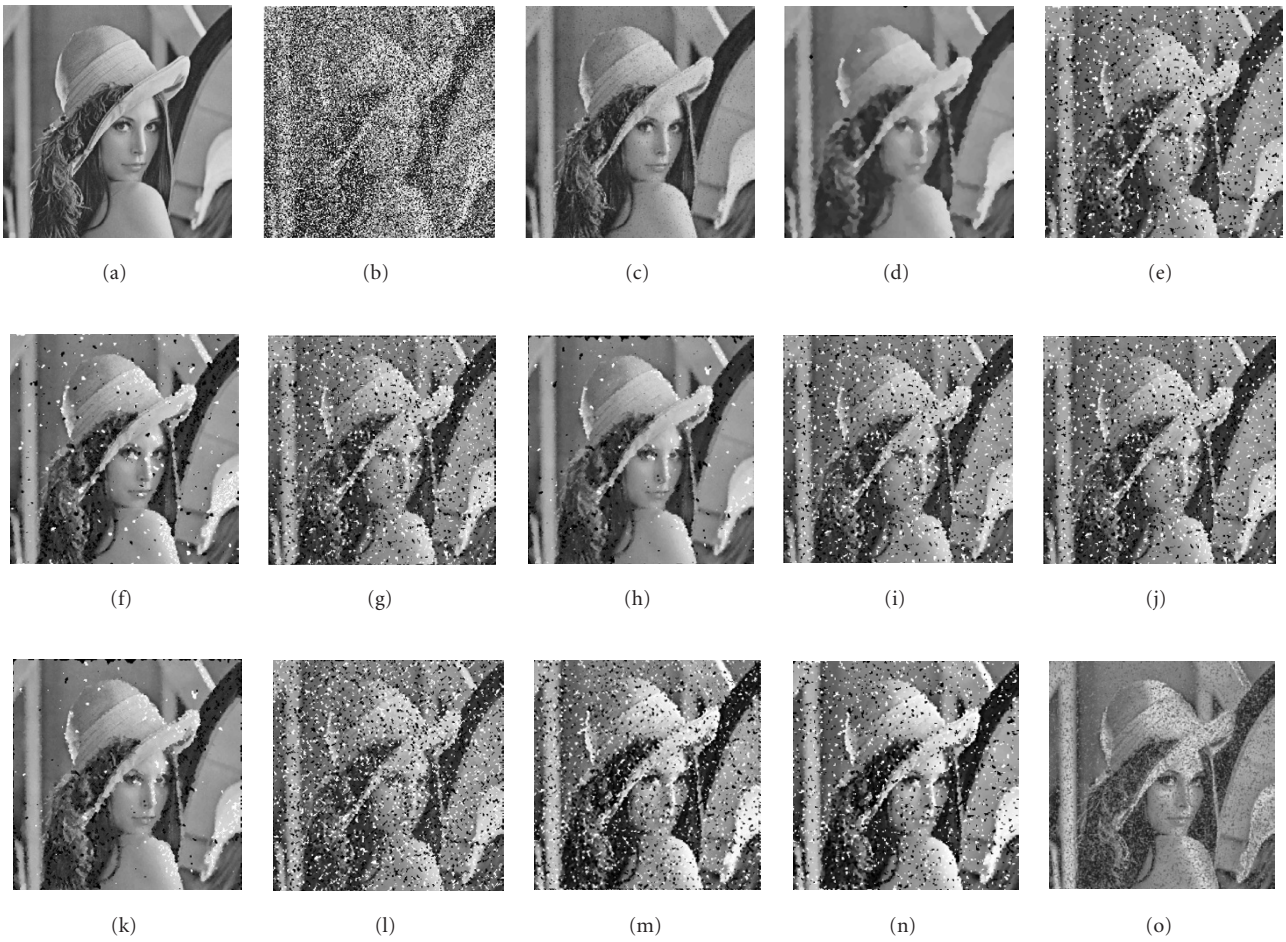

Figure 7: The restored images of noisy Lena for the noise density of 50%. (a) The original (noise-free) Lena, (b) noisy Lena for the noise density of 50%, (c) *Anfis-F* (proposed), (d) IMF, (e) SMF, (f) PSM, (g) SDROM, (h) SDROMR, (i) IRF, (j) ACWM, (k) ACWMR, (l) CWM, (m) CWMR, (n) SSMF, and (o) YUKSEL.

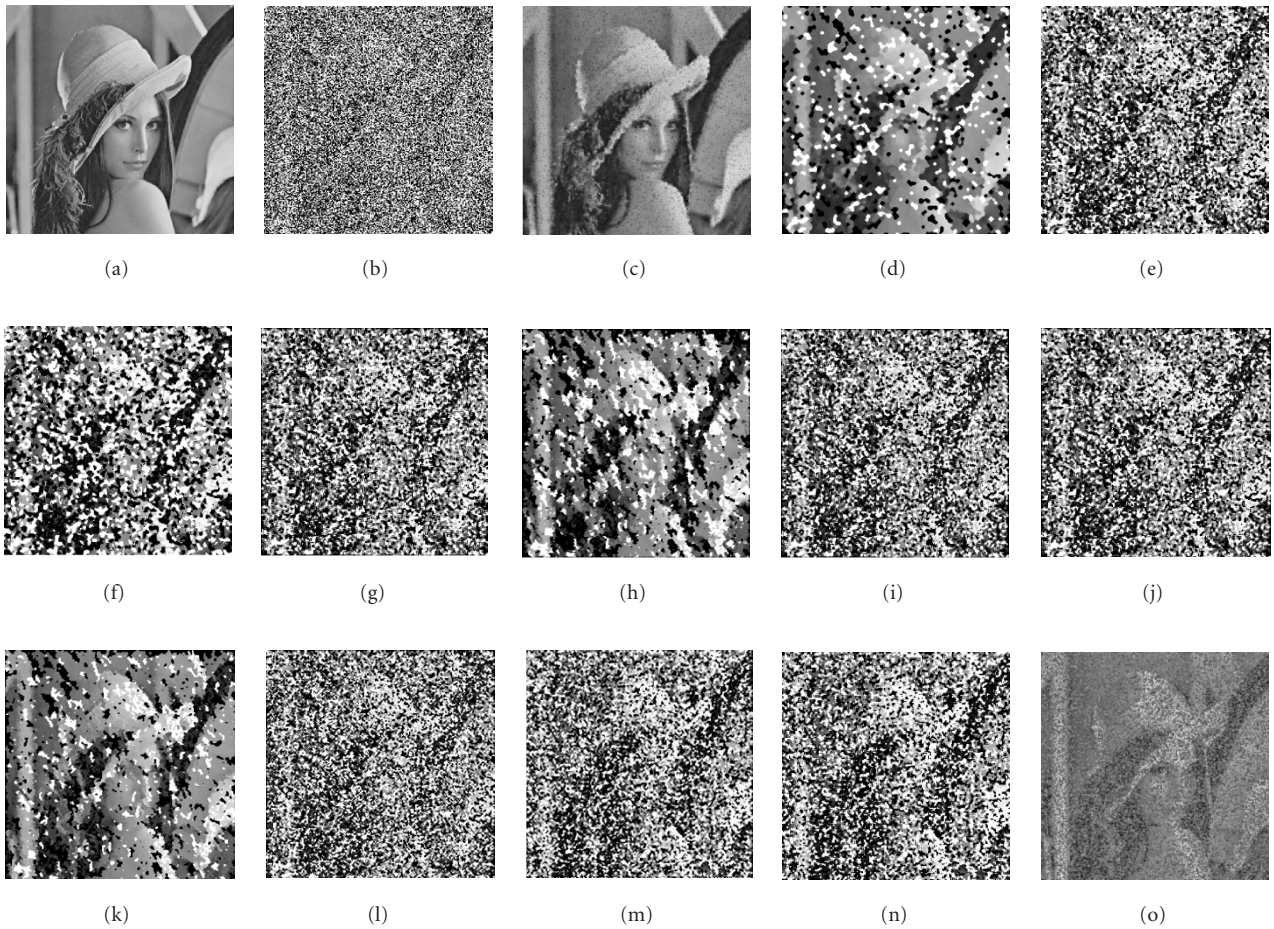

Figure 8: The restored images of noisy Lena for the noise density of 80%. (a) The original (noise-free) Lena, (b) noisy Lena for the noise density of 80%, (c) *Anfis-F* (proposed), (d) IMF, (e) SMF, (f) PSM, (g) SDROM, (h) SDROMR, (i) IRF, (j) ACWM, (k) ACWMR, (l) CWM, (m) CWMR, (n) SSMF, and (o) YUKSEL.

(iii) Set Delaunay triangulation network over the noisy image by using (x, y) values.

(iv) Delete the Delaunay triangles, which do not consist at least one corrupted pixel.

(v) Train the same Anfis structure for each Delaunay triangle using coordinates and intensity values of the corner nodes of the related Delaunay triangle.

(vi) Use the corresponding trained Anfis network to get the restored gray values of abnormally distributed pixels, which are suspected to be corrupted pixels.

(vii) Delete the padded pixels in order to obtain the restored image at the size of the original noisy image.

6. EXPERIMENTS

A number of experiments were achieved in order to evaluate the performance of the proposed *Anfis-F* in comparison with the recently introduced and highly approved filters. The experiments were carried out on the Lena, the Mandrill and the Peppers gray scale test images, which are 256×256 pixel-sized and 8 bits/pixel. The test images were corrupted by IN at various noise densities ranging from 10% to 90%. The restoration results of the Lena and the Mandrill images for the noise densities of 50% and 80% are illustrated in Figures 7–10 in order to evaluate the restoration performances of the mentioned methods subjectively. It is easily seen from Figures 7–10 that noise suppression and detail preservation are satisfactorily compromised by the proposed *Anfis-F*, especially when the noise density is very high. Restoration performances are objectively evaluated by using MSE, which is defined as

$$\mathrm{MSE} = \frac{1}{MN} \sum_{x=1}^{M} \sum_{y=1}^{N} \left(O_{x,y} - R_{x,y}\right)^2, \tag{8}$$

where $O_{x,y}$ and $R_{x,y}$ denote the original noise-free image pixels and the restored image pixels, respectively. M and N are the total number of pixels in the horizontal and vertical dimensions of the images. The major improvement achieved by the proposed *Anfis-F* has been demonstrated with extensive simulations of the mentioned test images corrupted at different noise densities.

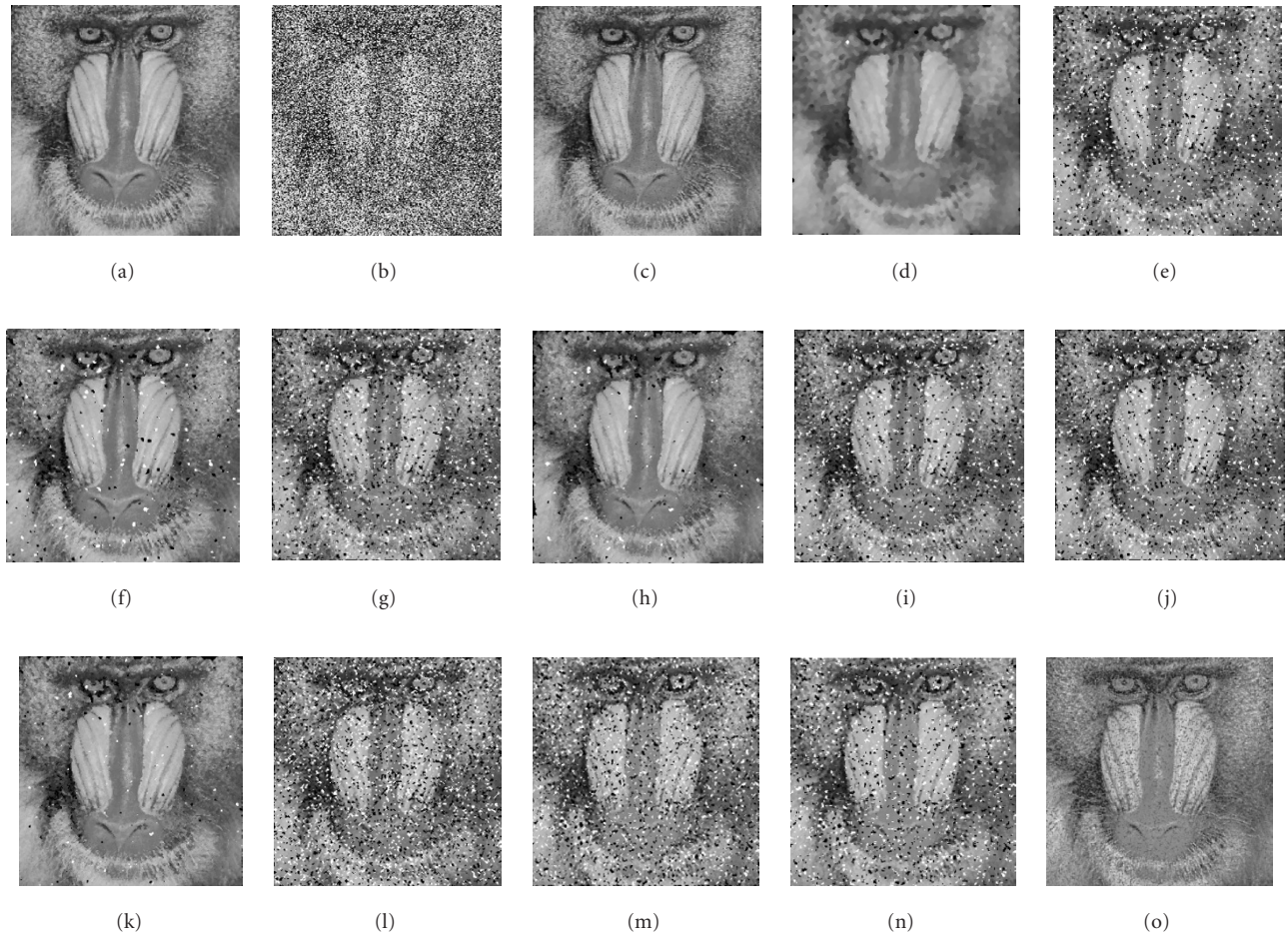

Figure 9: The restored images of noisy Mandrill for the noise density of 50%. (a) The original (noise-free) Mandrill, (b) noisy Mandrill for the noise density of 50%, (c) *Anfis-F* (proposed), (d) IMF, (e) SMF, (f) PSM, (g) SDROM, (h) SDROMR, (i) IRF, (j) ACWM, (k) ACWMR, (l) CWM, (m) CWMR, (n) SSMF, and (o) YUKSEL.

The IMF, SMF, PSM, SDROM, SDROMR, IRF, ACWM, ACWMR, CWM, CWMR, SSMF, and YUKSEL have been simulated as well for performance comparison. The restoration performances of the mentioned methods in MSE have been listed in Tables 1, 2, and 3, where it is obviously seen that the proposed *Anfis-F* provides a substantial improvement compared with the simulated filters, especially at the high noise density values. The IN removal and detail preservation are best compromised by the proposed *Anfis-F*. Robustness is one of the most important requirements of modern image enhancement filters and Tables 1, 2, and 3 indicate that the proposed *Anfis-F* provides robustness substantially across a wide variation of noise densities.

The average runtimes of all the mentioned filters were also determined and given in Table 4 in order to appreciate the computational complexities. These average values were obtained by running the algorithms 20 times and calculating the arithmetic means of the runtimes for each of the filters. The runtime analysis of the proposed *Anfis-F* filter and concerned filters were conducted for test images using Pentium IV, 1.1 GHz PC and documented in Table 4.

Table 4: Average runtimes of mentioned methods obtained by using Matlab.

Method	Average runtime (s)
Anfis-F	21.45
IMF	0.71
SMF	0.37
PSM	476.87
SDROM	4.26
SDROMR	5.76
IRF	12.50
ACWM	7.76
ACWMR	520.78
CWM	3.76
CWMR	150.92
SSMF	470.96
YUKSEL	4.90

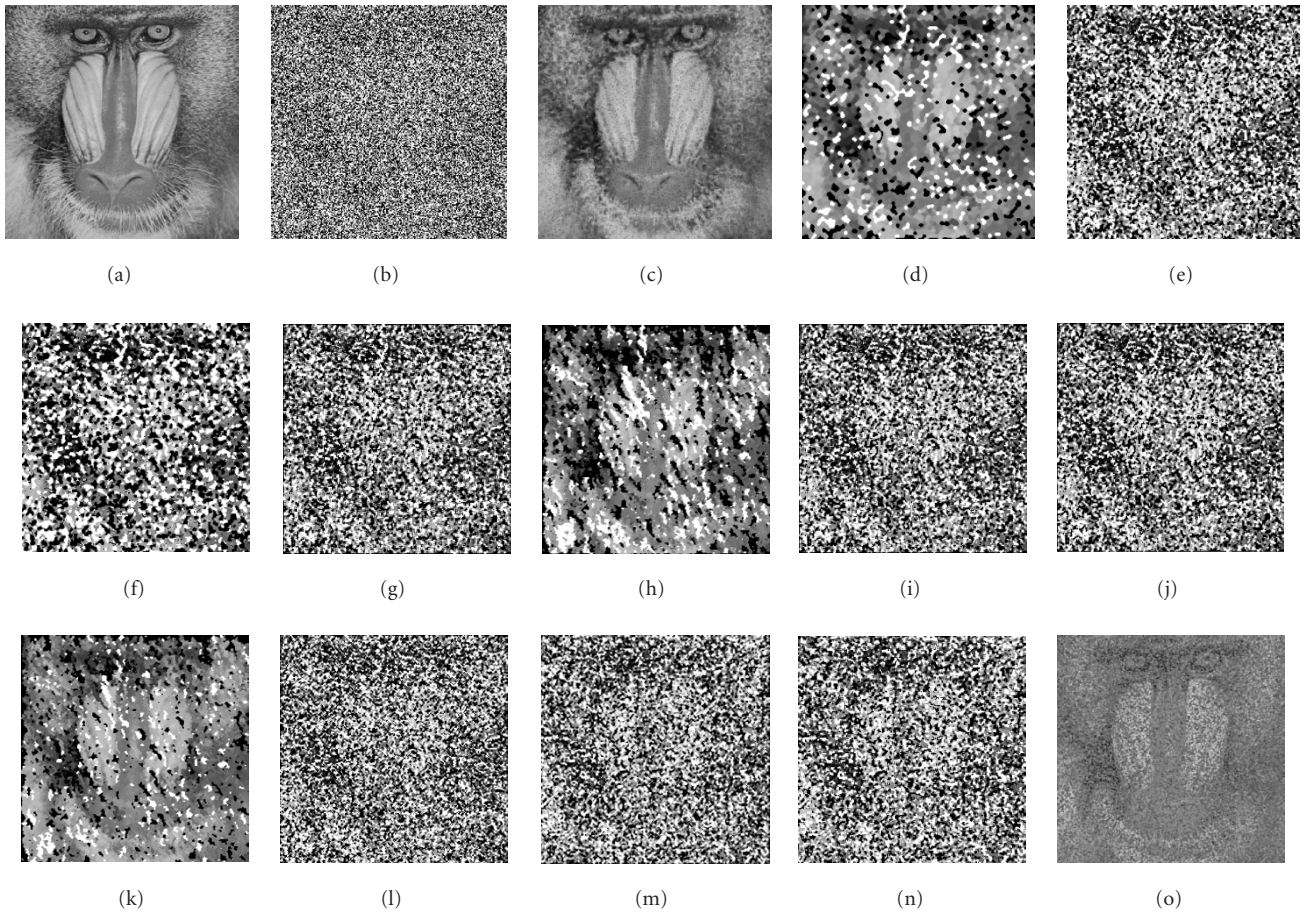

FIGURE 10: The restored images of noisy Mandrill for the noise density of 80%. (a) The original (noise-free) Mandrill, (b) noisy Mandrill for the noise density of 80%, (c) *Anfis-F* (proposed), (d) IMF, (e) SMF, (f) PSM, (g) SDROM, (h) SDROMR, (i) IRF, (j) ACWM, (k) ACWMR, (l) CWM, (m) CWMR, (n) SSMF, and (o) YUKSEL.

7. CONCLUSIONS

In this paper, a new and efficient Anfis-based IN elimination filter, *Anfis-F*, is introduced. The effectiveness of the proposed filter in processing different images can easily be evaluated by appreciating Tables 1, 2, and 3, which are given to present the restoration results of *Anfis-F* and the comparison filters for images degraded by IN, where noise density ranges from 10% to 90%. It is seen from Tables 1, 2, and 3 that the proposed *Anfis-F* gives absolutely better restoration results and a higher resolution in the restored images than the comparison filters, IMF, SMF, PSM, SDROM, SDROMR, IRF, ACWM, ACWMR, CWM, CWMR, SSMF, and YUKSEL. Compared with the other filters, the proposed *Anfis-F* yields satisfactory results in suppressing IN while requiring a simple computational structure. In addition, the proposed *Anfis-F* supplies more pleasing restoration results aspect of visual perception and also provides the best tradeoff between IN suppression and image enhancement for detail preservation as seen in Figures 7–10.

The advantages of the proposed filter may be summarized as follows.

(i) The proposed method uses Delaunay triangles as finite elements, therefore it requires training Anfis structures. This is a new approach for Anfis-based applications and it is obviously seen from Tables 1, 2, and 3 that the proposed method supplies superior restoration results to the comparison filters.

(ii) *Anfis-F* supplies visually pleasing images even if the noise density is very high, whereas others do not supply visually pleasing images when the noise density is higher than 50%.

(iii) In order to find the corrupted pixels more accurately, the proposed method uses lillietest, which is known as a powerful tool for normality test of samples.

(iv) *Anfis-F* needs training many artificial soft computing structures (in this paper Anfis structures), as in [35], but it guarantees superior restoration results as seen in Tables 1, 2, and 3.

(v) The proposed method uses simple triangular membership functions and linear function at the inputs and output of the Anfis structures, respectively, in order to simplify computational requirements.

REFERENCES

[1] J. W. Tukey, "Nonlinear (nonsuperposable) methods for smoothing data," in *Proc. IEEE Electronws and Aerospace Systems Convention (Cong. Rec. EASCON' 74)*, p. 673, Washington, DC, USA, 1974.

[2] Z. Wang and D. Zhang, "Progressive switching median filter for the removal of impulse noise from highly corrupted images," *IEEE Trans. on Circuits and Systems II: Analog and Digital Signal Processing*, vol. 46, no. 1, pp. 78–80, 1999.

[3] A. Rodríguez-Vázquez, S. Espejo, R. Domínguez-Castro, R. Carmona, and G. Liñán, "CMOS design of focal plane programmable array processors," in *Proc. European Symposium on Artificial Neural Networks*, pp. 57–62, Bruges, Belgium, April 2001.

[4] T. Chen and H. R. Wu, "Adaptive impulse detection using center-weighted median filters," *IEEE Signal Processing Letters*, vol. 8, no. 1, pp. 1–3, 2001.

[5] E. Abreu, M. Lightstone, S. K. Mitra, and K Arakawa, "A new efficient approach for the removal of impulse noise from highly corrupted images," *IEEE Trans. Image Processing*, vol. 5, no. 6, pp. 1012–1025, 1996.

[6] S.-J. Ko and Y. H. Lee, "Center weighted median filters and their applications to image enhancement," *IEEE Trans. Circuits and Systems*, vol. 38, no. 9, pp. 984–993, 1991.

[7] T. Chen and H. R. Wu, "A new class of median based impulse rejecting filters," in *IEEE International Conference on Image Processing*, vol. 1, pp. 916–919, Vancouver, BC, Canada, September 2000.

[8] W.-Y. Han and J.-C. Lin, "Minimum-maximum exclusive mean (MMEM) filter to remove impulse noise from highly corrupted images," *Electronics Letters*, vol. 33, no. 2, pp. 124–125, 1997.

[9] M. Muneyasu, N. Nishi, and T. Hinamoto, "A new adaptive center weighted median filter using counter propagation networks," *Journal of the Franklin Institute*, vol. 337, pp. 631–639, 2000.

[10] G. Pok, J.-C. Liu, and A. S. Nair, "Selective removal of impulse noise based on homogeneity level information," *IEEE Trans. Image Processing*, vol. 12, no. 1, pp. 85–92, 2003.

[11] M. E. Yüksel and A. Baştürk, "Efficient removal of impulse noise from highly corrupted digital images by a simple neuro-fuzzy operator," *AEÜ International Journal of Electronics and Communications*, vol. 57, no. 3, pp. 214–219, 2003.

[12] F. Russo, "Edge detection in noisy images using fuzzy reasoning," *IEEE Trans. Instrumentation and Measurement*, vol. 47, no. 5, pp. 1102–1105, 1998.

[13] F. Russo and G. Ramponi, "A fuzzy filter for images corrupted by impulse noise," *IEEE Signal Processing Letters*, vol. 3, no. 6, pp. 168–170, 1996.

[14] F. Russo, "Evolutionary neural fuzzy systems for noise cancellation in image data," *IEEE Trans. Instrumentation and Measurement*, vol. 48, no. 5, pp. 915–920, 1999.

[15] D. Zhang and Z. Wang, "Impulse noise detection and removal using fuzzy techniques," *Electronics Letters*, vol. 33, no. 5, pp. 378–379, 1997.

[16] J.-H. Wang, W.-J. Liu, and L.-D. Lin, "Histogram-based fuzzy filter for image restoration," *IEEE Trans. Systems, Man, and Cybernetics, Part B*, vol. 32, no. 2, pp. 230–238, 2002.

[17] J. S. R. Jang, "Anfis: adaptive-network-based fuzzy inference system," *IEEE Trans. Systems, Man, and Cybernetics*, vol. 23, no. 3, pp. 665–685, 1993.

[18] J. S. R. Jang, C. T. Sun, and E. Mizutani, *Neuro-Fuzzy and Soft Computing: A Computational Approach to Learning and Machine Intelligence*, Prentice-Hall, Upper Saddle River, NJ, USA, 1997.

[19] K. Pal and S. Mitra, "Multilayer perceptron, fuzzy sets, and classification," *IEEE Transactions on Neural Networks*, vol. 3, no. 5, pp. 683–697, 1992.

[20] H. Takagi and M. Sugeno, "Fuzzy identification of systems and its applications to modeling and control," *IEEE Trans. Systems, Man, and Cybernetics*, vol. 15, no. 1, pp. 116–132, 1985.

[21] H. Takagi and I. Hayashi, "NN-driven fuzzy reasoning," *International Journal of Approximate Reasoning*, vol. 5, no. 3, pp. 191–212, 1991.

[22] L. Zadeh, "Fuzzy sets," *Information and Control*, vol. 8, no. 3, pp. 338–353, 1965.

[23] S. Haykin, *Neural Networks: A Comprehensive Foundation*, Macmillian College Publishing, New York, NY, USA, 1994.

[24] Y. Hayashi, J. J. Buckley, and E. Czogala, "Fuzzy neural network with fuzzy signals and weights," *International Journal of Intelligent Systems*, vol. 8, no. 4, pp. 527–537, 1993.

[25] MathWorks, "MATLAB the language of technical computing," *MATLAB Function Reference*, MathWorks, New York, 2002.

[26] F. P. Preparata and M. I. Shamos, *Computational Geometry: An Introduction*, Springer-Verlag, New York, NY, USA, 1985.

[27] S. Price, "Surface interpolation of apartment rental data: can surfaces replace neighborhood mapping," *The Appraisal Journal*, vol. 70, no. 3, pp. 260–273, 2002.

[28] L. J. Guibas, D. E. Knuth, and M. Sharir, "Randomized incremental construction of Delaunay and Voronoi diagrams," *Algorithmica*, vol. 7, no. 4, pp. 381–413, 1992.

[29] D. F. Watson, *Contouring: A Guide to the Analysis and Display of Spatial Data*, Pergamon Press, New York, NY, USA, 1992.

[30] T. Y. Yang, *Finite Element Structural Analysis*, Prentice-Hall, Englewood Cliffs, NJ, USA, 1986.

[31] C. L. Brown and A. M. Zoubir, "Testing for impulsive behavior: a bootstrap approach," *Digital Signal Processing*, vol. 11, no. 2, pp. 120–132, 2001.

[32] Bestfit, *Probability distribution fitting for Microsoft windows,* Software, version 4.5.2, Palisade Co., UK, 2002.

[33] MathWorks, "MATLAB the language of technical computing," *MATLAB Statistics Toolbox User Guide*, MathWorks, New York, 2003.

[34] W. Conover, *Practical Nonparametric Statistics*, John Wiley & Sons, New York, NY, USA, 2nd edition, 1980.

[35] G. K. Knopf and J. Kofman, "Adaptive reconstruction of free-form surfaces using Bernstein basis function networks," *Engineering Applications of Artificial Intelligence*, vol. 14, no. 5, pp. 577–588, 2001.

Erkan Beşdok was born in 1969 in Kayseri, Turkey. He received the B.S., M.S., and Ph.D. degrees from Istanbul Technical University, Istanbul, Turkey, all in geodesy and photogrammetry engineering. He is now an Assistant Professor with the Erciyes University, Engineering Faculty, Geodesy and Photogrammetry Engineering Department and Institute of Science, Computer Engineering Department. His current research interests are computer vision, photogrammetric image processing, medical imaging, information visualization, neural networks, fuzzy sets and systems, genetics, ant colony theory, and information systems.